ACS Chemical Neuroscience

Research Article

pubs.acs.org/chemneuro

Adsorption of α-Synuclein to Supported Lipid Bilayers: Positioning and Role of Electrostatics

Erik Hellstrand,*[,†] Marie Grey,[‡] Marie-Louise Ainalem,[§] John Ankner,[∥] V. Trevor Forsyth,[⊥,○] Giovanna Fragneto,[⊥] Michael Haertlein,[⊥] Marie-Therese Dauvergne,[⊥] Hanna Nilsson,[†] Patrik Brundin,[@,#] Sara Linse,[▽] Tommy Nylander,[‡] and Emma Sparr[‡]

[†]Biophysical Chemistry, Department of Chemistry, Lund University, SE-22100 Lund, Sweden

[‡]Physical Chemistry, Department of Chemistry, Lund University, SE-22100 Lund, Sweden

[§]European Spallation Source ESS, SE-22100 Lund, Sweden

[∥]Oak Ridge National Laboratory, Spallation Neutron Source, Oak Ridge, Tennessee 37831, United States

[⊥]Institut Laue-Langevin, 6, rue Jules Horowitz, 38042 Grenoble, France

[@]Neuronal Survival Unit, Wallenberg Neuroscience Center, Lund University, BMC B11, 221 84 Lund, Sweden

[#]Center for Neurodegenerative Science, Van Andel Research Institute, 333 Bostwick Avenue Northeast, Grand Rapids, Michigan 49503, United States

[▽]Biochemistry and Structural Biology, Department of Chemistry, Lund University, SE-22100 Lund, Sweden

[○]EPSAM/ISTM, Keele University, Staffordshire, ST5 5BG, UK

Supporting Information

ABSTRACT: An amyloid form of the protein α-synuclein is the major component of the intraneuronal inclusions called Lewy bodies, which are the neuropathological hallmark of Parkinson's disease (PD). α-Synuclein is known to associate with anionic lipid membranes, and interactions between aggregating α-synuclein and cellular membranes are thought to be important for PD pathology. We have studied the molecular determinants for adsorption of monomeric α-synuclein to planar model lipid membranes composed of zwitterionic phosphatidylcholine alone or in a mixture with anionic phosphatidylserine (relevant for plasma membranes) or anionic cardiolipin (relevant for mitochondrial membranes). We studied the adsorption of the protein to supported bilayers, the position of the protein within and outside the bilayer, and structural changes in the model membranes using two complementary techniques—quartz crystal microbalance with dissipation monitoring, and neutron reflectometry. We found that the interaction and adsorbed conformation depend on membrane charge, protein charge, and electrostatic screening. The results imply that α-synuclein adsorbs in the headgroup region of anionic lipid bilayers with extensions into the bulk but does not penetrate deeply into or across the hydrophobic acyl chain region. The adsorption to anionic bilayers leads to a small perturbation of the acyl chain packing that is independent of anionic headgroup identity. We also explored the effect of changing the area per headgroup in the lipid bilayer by comparing model systems with different degrees of acyl chain saturation. An increase in area per lipid headgroup leads to an increase in the level of α-synuclein adsorption with a reduced water content in the acyl chain layer. In conclusion, the association of α-synuclein to membranes and its adsorbed conformation are of electrostatic origin, combined with van der Waals interactions, but with a very weak correlation to the molecular structure of the anionic lipid headgroup. The perturbation of the acyl chain packing upon monomeric protein adsorption favors association with unsaturated phospholipids preferentially found in the neuronal membrane.

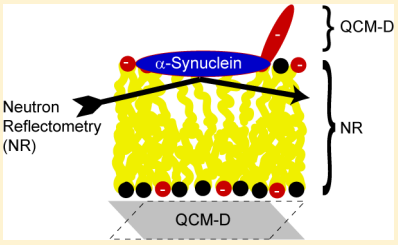

KEYWORDS: *Parkinson, Lewy body, bilayer, α-synuclein, amyloidosis, neutron diffraction, perdeuterated protein*

The synaptic protein α-synuclein is implicated in Parkinson's disease (PD), the second most common neurodegenerative disease.[1] PD can cause motor symptoms, cognitive impairment, and an array of other nonmotor symptoms.[2] In addition to gene duplication and triplication, three point mutations in the α-synuclein gene sequence are linked to early onset PD.[3−7] Certain single-nucleotide polymorphisms in the gene are also associated with an increased risk of disease. In PD, neurons progressively perish in several brain regions. One of the most affected is called the *substantia nigra*, and its degeneration probably underlies most of the motor symptoms of PD. These neurons contain characteristic inclusions called Lewy bodies (LBs), which are protein aggregates mainly comprised of α-synuclein, but lipids are also present.[8,9] α-Synuclein has a high aggregation propensity,

Received: March 18, 2013
Accepted: July 3, 2013
Published: July 3, 2013

and formation of ordered α-synuclein aggregates (fibrils) correlates with neurodegeneration *in vivo*. It has also been suggested that fibrils are neuroprotective, and that smaller aggregates, oligomers, are most toxic.[10−12]

In LBs, the 140-amino acid α-synuclein is present in an aggregated, β-sheet rich conformation. In solution, monomeric α-synuclein is a largely unstructured protein, sometimes termed an intrinsically disordered protein or natively unfolded protein. Recently, post-translationally modified α-synuclein was proposed to exist in a tetrameric state *in vivo*, although the relevance and occurrence of this form have been debated in other studies.[13,14] Therefore, isolation of a monomer to obtain a well-defined starting state is preferred for *in vitro* studies. Membrane-associated α-synuclein is found to contain α-helices, and β-sheet structures appear as the protein aggregates.[15−17]

While the normal function of α-synuclein *in vivo* is poorly understood, it appears to play a role in regulating synaptic vesicle recycling.[18] The N-terminal portion of the protein is proposed to be responsible for the protein−lipid interaction. This is also supported by the sequence as it contains an imperfect repeat found in other proteins binding lipids reversibly.[19] The C-terminal part, on the other hand, is highly negatively charged and proposed to be responsible for protein−protein interactions,[20] whereas the middle hydrophobic part is essential for forming β-sheets during aggregation.[21]

The interaction between α-synuclein and lipid membranes has been intensively studied in recent years. Interestingly, α-synuclein variants with early onset mutations have different membrane binding affinity.[22,23] According to the "prion-like" hypothesis, misfolded α-synuclein might transfer between neurons and seed aggregation in the recipient cells.[24] The intercellular transfer of α-synuclein has been suggested to be most efficient when it is bound to exosomes,[25,26] which are small vesicles formed by budding of the cell membrane. Cell stress, leading to the overloading of the lysosomal system, is suggested to increase the transfer of α-synuclein via these exosome vesicles.[27] Structural details of the interaction of α-synuclein with membranes are still scarce, but previous studies have suggested that α-synuclein penetrates up to 14 Å into the outer leaflet of anionic bilayers, with a considerable portion of the membrane-bound protein extending into the solvent.[28−30]

In this study, the adsorption of α-synuclein to negatively charged or zwitterionic phospholipid bilayers was investigated using quartz crystal microbalance with dissipation monitoring (QCM-D) and neutron reflectivity (NR). QCM-D provides information about the total amount of material, including coupled solvent, attached to the surface from the change in frequency as well as the viscoelastic properties of the attached layer from the dissipation. To determine the changes in adsorbed layer composition upon protein adsorption and the depth of penetration of the adsorbed protein into the bilayer and to study the response in the supported bilayer, we used NR. This technique provides detailed structural information perpendicular to an interface and can thus provide information about both protein penetration depth and changes in the bilayer density and thickness resulting from α-synuclein association. We have chosen lipid systems that are highly relevant for PD, and we have systematically investigated how the tuning of electrostatic interactions affects protein binding. The investigated lipids are phosphatidylcholine (PC) together with phosphatidylserine (PS), found in the cell membrane, and cardiolipin (CL), found in the mitochondrial membrane. Mitochondrial dysfunction is suggested to be involved in PD pathogenesis, and the amount of α-synuclein associated to mitochondria is increased in the *substantia nigra* of PD patients.[31]

RESULTS

Model Membrane. We have characterized association of the α-synuclein monomer to deposited lipid bilayers composed of (1) pure PC, (2) PC mixed with 30 mol % phosphatidylserine (PS), or (3) PC mixed with 15 mol % CL. Palmitoyloleoyl (PO) or dioleoyl (DO) chains were chosen so that the lipid bilayers correspond to the liquid disordered lamellar phase under the conditions described here, making them a simple model of cell membranes. With regard to lipid headgroups, zwitterionic PC is the most abundant phospholipid in human cell membranes and PS is the most common anionic phospholipid, localized in the inner leaflet of cell membranes.[32−34] Furthermore, CL is a major component of the mitochondrial membrane[33] and carries two anionic phosphatidyl residues connected by a glycerol bridge and four acyl chains. Mitochondria have recently attracted interest as potential actors in the pathogenesis of PD.[31,35] Therefore, these types of lipids were chosen for this study. The average charge density is expected to be the same for the studied anionic bilayers with 30% PS or 15% CL (see Discussion for further details).

Extending Protein Film Analyzed by QCM-D. QCM-D has been proven to be a useful technique for studying bilayer deposition and protein binding to lipid membranes as the technique provides information about both the amount that can be expressed as the layer thickness and the viscoelastic properties of the layer.[36,37] Here, QCM-D was used to obtain a quantitative measure of the adsorption of monomeric α-synuclein to deposited POPC, 70:30 POPC/DOPS, or 85:15 POPC/CL bilayers from solutions with different pH values and electrolyte concentrations. The three different buffer solutions tested consisted of 10 mM MES buffer (pH 5.5), 10 mM MES buffer (pH 5.5) with 150 mM NaCl, and 10 mM HEPES buffer (pH 7.0). Control experiments in phosphate buffer produced similar results (data not shown). Figure 1 shows the QCM-D data recorded during injection of 4 μM monomeric α-synuclein freshly isolated by size exclusion chromatography. Time zero corresponds to the start of injection, and it takes approximately 2.5 min for the injected solution to reach the measuring cell. In the cases where adsorption is detected, i.e., when the frequency and dissipation display shifts after injection, the changes in measured parameters are almost instantaneous. This suggests fast association kinetics within the time frame of the mixing process in the flow cell. The total time of injection was 10−15 min, and the subsequent dissociation from the lipid bilayer (desorption), was much slower than the adsorption (Figure S1 of the Supporting Information).

A typical frequency shift divided by the overtone number for bilayer deposition was 26 Hz and corresponds to an adsorbed amount of 460 ng/cm^2. Using a density of 1, this corresponds to a thickness of 46 Å, if full coverage is reached. A typical deposited liquid crystalline phase bilayer composed of phospholipids with C18:1 acyl chains has a thickness of 40 Å,[38,39] and the surface coverage of the deposited layers is most often <100%. The reason for this apparent divergence is that QCM-D measures the "wet mass", which includes acoustically coupled water molecules. Because of the inclusion of the coupled water, QCM-D can be regarded as a type of hydrodynamic measurement, similar to the hydrodynamic size

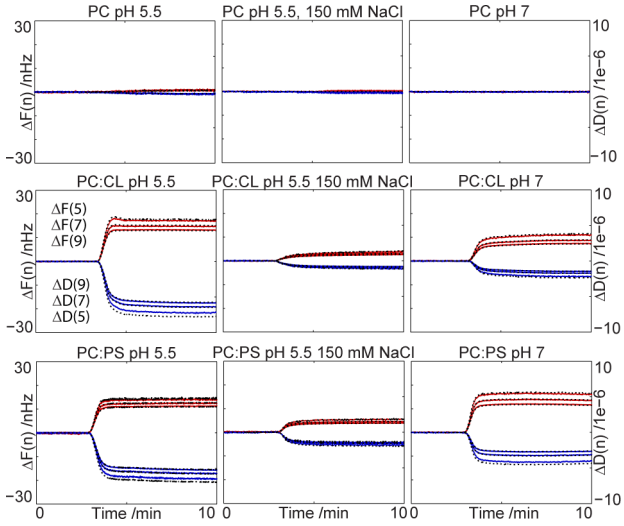

Figure 1. Adsorption of α-synuclein to supported lipid bilayers is sensitive to bilayer charge and solution conditions. Frequency (blue) and dissipation (red) for overtone numbers 5, 7, and 9, monitored via QCM-D, upon injection of 4 μM α-synuclein to phospholipid bilayers deposited on SiO_2-coated quartz crystals under different solution conditions. No or little adsorption is seen for the pure POPC bilayers (top), while significant adsorption to DOPS-containing (middle) or CL-containing (bottom) bilayers is observed. Injection is started at time zero, and the protein reaches the bilayer in the flow cell after approximately 2.5 min. Black lines show the fitted Voight model presented in Figure 2.

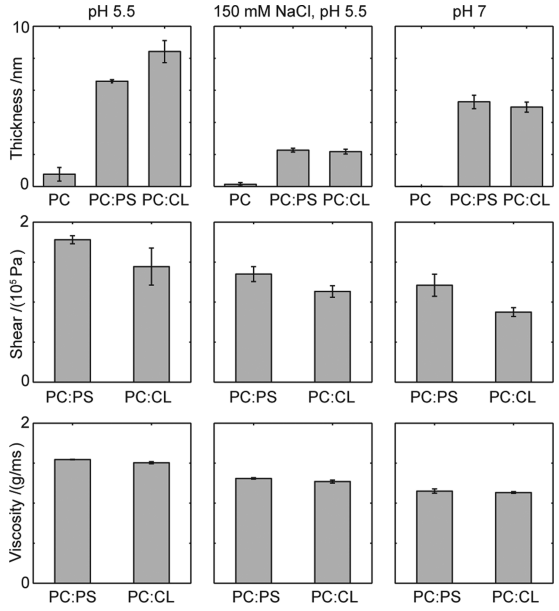

Figure 2. Thickness (top), shear (middle), and viscosity (bottom) obtained from a fitted Voight model to the QCM-D data for the protein film extending from the bilayer. Error bars indicate the standard error equivalent to a 68% confidence interval for two to four parallel measurements with individual model fitting. Typical raw data used in the modeling are presented in Figure 1.

determined using dynamic light scattering.[38] The lipid bilayer is dense and homogeneous enough to allow for use of the Sauerbrey equation; i.e., it has a rather low degree of acoustic coupling to the surrounding medium.[40] When the protein adsorbs to the bilayer, the shift and dissipation for the different overtones as measured in the QCM-D experiment are not the same (Figure 1). The discrepancy between data recorded at different overtones reveals that the adsorbed film is viscoelastic.[38] The response in frequency is therefore not directly proportional to the adsorbed mass as depicted with the Sauerbrey equation but needs to be analyzed together with the dissipation, using a viscoelastic model.

Figure 2 shows the thickness, shear modulus, and viscosity of the protein film extending from the bilayer. Data were obtained using a Voight representation of a viscoelastic film[38,41] fitted to overtone numbers 5, 7, and 9 and are shown as black lines in Figure 1. From the top panels in Figure 2, it is clear that the thickest protein film extending from the bilayer is observed for anionic bilayers at pH 5.5 (9 nm for 85:15 POPC/CL bilayers and 7 nm for 7:3 POPC/DOPS bilayers). Both bilayers have the same average charge density, but CL is expected to be effectively divalent, which can lead to stronger Coulomb interactions at short separations. The importance of electrostatic interactions is confirmed with the increase in the salt concentration to physiological levels, allowing more efficient screening of all electrostatic interactions. At pH 5.5 and 150 mM NaCl, the extending protein film is collapsed to only 2 nm, and no difference in QCM-D response is seen between the PS- and CL-containing bilayers. Increasing the pH to 7.0 at low salt concentrations results in a film with an intermediate thickness of 5 nm. For the bilayers composed of only zwitterionic POPC, there is only a minor amount of protein adsorbed at all pH values and electrolyte concentrations, resulting in poor modeling of the protein film.

The two bottom panels of Figure 2 show the shear modulus and viscosity of the modeled extending protein film. Only the anionic bilayers are analyzed because the adsorption to POPC bilayers was negligible. The shear modulus describes the shear stiffness of the film and consists of the storage modulus and the loss modulus, coupled to the viscosity. Both the shear modulus and viscosity show the same trends, and we can conclude that the most viscous films are produced at low pH values and low salt concentrations.

Position and Membrane Response from Neutron Reflectometry. The QCM-D study reveals key differences in adsorption of α-synuclein to supported bilayers depending on electrostatic conditions. However, because QCM-D is an acoustic technique, the results are significantly more sensitive to the protein film extending into the bulk outside the bilayer than the protein segments partitioning into the bilayer. We therefore use NR to gain deeper insight into α-synuclein adsorption and, in particular, more detailed information about where the protein is positioned in the bilayer and how the bilayer responds to protein adsorption. The lipid compositions chosen were those yielding the thickest and most rigid protein films by QCM-D, i.e., PC together with either 30% PS or 15% CL, to keep the net charge density constant. Because the largest responses were seen at pH 5.5 and low ionic strengths, this solution condition was used in the NR measurements. Low pH is furthermore associated with PD through both the exosomes via the lysosomal pathway[42] and oxidative or metabolic stress in mitochondria.[43]

The contrast in NR is determined by the differences in the scattering length density (SLD) values for the various sample components. Hydrogen and deuterium have markedly different SLD values, and with a change in the degree of deuteration of lipids, protein, and solvent, the contribution from the different

dx.doi.org/10.1021/cn400066t | ACS Chem. Neurosci. 2013, 4, 1339−1351

components to neutron scattering of a sample can be matched so that the scattering from a specific part, region, or component of interest is highlighted. The bilayers were deposited in exactly the same way as in the QCM-D studies but on silicon supports featuring 14 Å thin silicon oxide layers. In contrast to QCM-D, NR was not conducted in real time during flow, but measurements were undertaken before bilayer deposition, after bilayer deposition, and after protein injection. The PC used had a perdeuterated palmitoyl chain (*d*-POPC), and the *α*-synuclein was perdeuterated (*d*-*α*-synuclein) in the neutron experiments while the charged lipids were kept hydrogenated. Figure 3 and Figure S2 of the Supporting Information illustrate

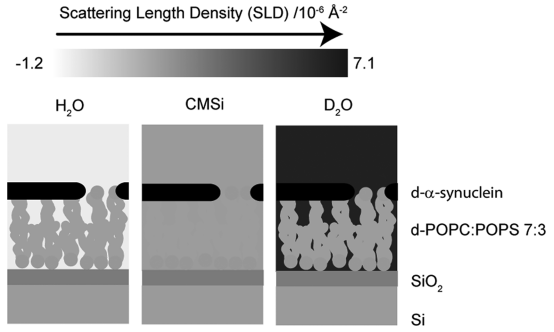

Figure 3. Illustration of the resulting SLD distribution in a 7:3 *d*-POPC/POPS bilayer with *d*-*α*-synuclein. See Figure S2 of the Supporting Information for corresponding illustrations of the other bilayers studied via NR.

the resulting SLD distribution in the experimental system. This combination of compounds with different degrees of deuteration has two advantages. One is that the acyl chains of *d*-POPC and the charged lipids have sufficiently different SLD values to allow detailed analysis of any asymmetry in the bilayer deposition. The other advantage is that the bilayer has an SLD value similar to that of the silicon substrate underneath the thin SiO_2 film. This gives high sensitivity in the reflectivity profile for the distance between the protein and the silicon oxide layer, i.e., the depth of penetration of the protein into the lipid bilayer.

Figure 4 shows NR data for the two different types of anionic bilayers in buffer solution with three different solvent contrasts, D_2O, CMSi, and H_2O. Table 1 presents the parameters for the fitted bilayer models from Figure 4. For a further description of the calculated values and the fitting procedure, see Methods and Table S1 of the Supporting Information. The fitted model parameters are in good agreement with those of deposited bilayers with similar compositions from previous studies.[44]

Table 1. Parameters Obtained from Layered Model Fits to NR Profiles Recorded for the Surface Deposition of Phospholipid Bilayers (i.e., the profiles presented in Figures 4 and 8)[a]

	thickness (Å)		
	headgroup region	acyl chain region	coverage (%)
7:3 *d*-POPC/POPS	5 ± 0.5	30 ± 0.5	82 ± 1
85:15 *d*-POPC/CL	5 ± 0.5	28 ± 0.5	83 ± 2
7:3 DOPC/DOPS	5 ± 0.5	30 ± 0.5	75 ± 1

[a]See Methods and Table S1 of the Supporting Information for further details of the fitting procedure and error analysis.

On the basis of available phase diagrams for PC/PS mixtures and PE/CL mixtures, showing miscibility of the lipids above the melting temperature,[45−47] the bilayers are expected to be laterally uniform. No macroscopic phase separation was observed in giant unilamellar vesicles with similar lipid compositions.[48] Lipid asymmetry between the two leaflets in mixed bilayer systems was recently reported for bilayers deposited by osmotic shock from 3:1 POPC/POPS vesicles where the initial vesicle adsorption took place in buffer solutions containing 1.1 M NaCl.[49] For the bilayers in Figure 4, simultaneous fitting of the SLD values in the inner and outer

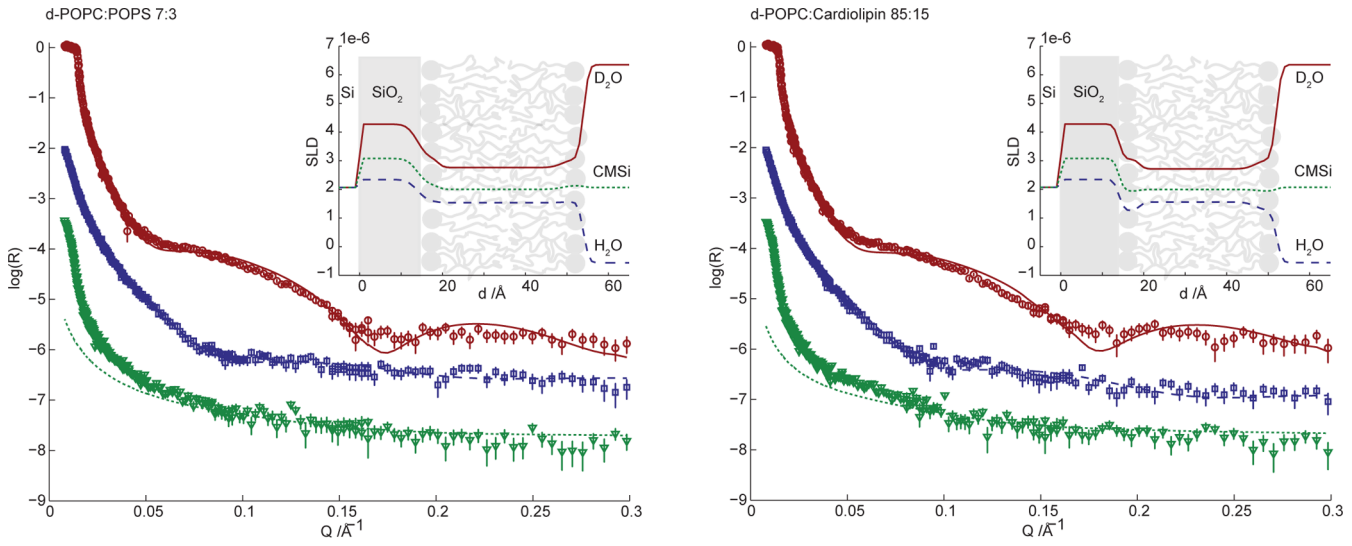

Figure 4. Neutron reflectivity (plotted as $\log_{10} R$) as a function of momentum transfer (Q) for surface-deposited 7:3 *d*-POPC/POPS (left) and 85:15 *d*-POPC/CL (right) phospholipid bilayers. The lines correspond to the fit of the multilayer models presented in Table 1 (fitting parameters in Table S1 of the Supporting Information). The reflectivity was measured for three degrees of solvent deuteration: D_2O (red circles, top curve), CMSi (green triangles, bottom curve), and H_2O (blue squares, middle curve). The deviation at low Q for CMSi originates from the instrumental setup and was disregarded during the modeling. Data in CMSi and H_2O are offset in $\log(R)$ by −2 and −1, respectively, for the sake of clarity. The insets show the resulting SLD profiles as a function of distance from the silicon substrate.

dx.doi.org/10.1021/cn400066t | *ACS Chem. Neurosci.* 2013, 4, 1339−1351

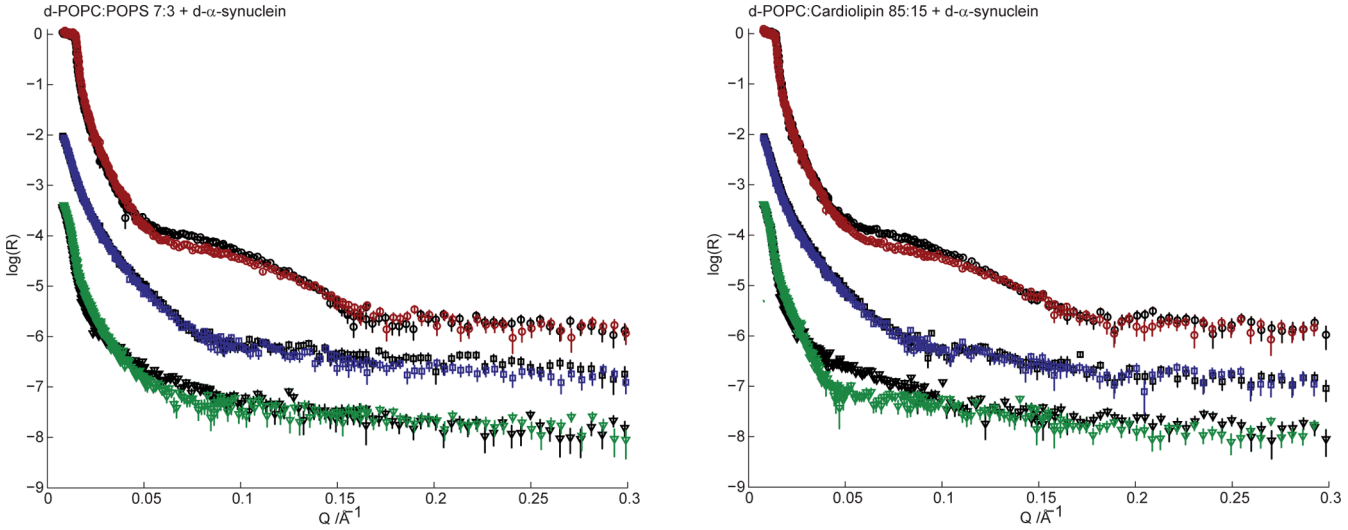

Figure 5. Neutron reflectivity (plotted as $\log_{10} R$) as a function of momentum transfer (Q) for surface-deposited 7:3 *d*-POPC/POPS (left) and 85:15 *d*-POPC/CL (right) phospholipid bilayers in the absence (black, Figure 4) and presence (color) of 4 μM *d*-α-synuclein. Reflectivity was measured for three solvent contrasts: D_2O (red circles), CMSi (green triangles), and H_2O (blue squares). CMSi and H_2O profiles are offset in $\log(R)$ by -2 and -1, respectively, for the sake of clarity.

acyl chain regions did not reveal any asymmetry with enrichment of anionic lipids in the outer leaflet of the bilayer. The analysis also reveals that there is no depletion of anionic phospholipids in the deposited bilayer compared to the injected vesicle solution. A symmetric model with two identical monolayers was thus used in the fitting procedure. The observed differences between the bilayers described here and the previously described asymmetric bilayers can be explained by the use of significantly different preparation and deposition methods.

Upon injection of *d*-α-synuclein, all reflectivity profiles change compared to those recorded in the absence of protein. Figure 5 presents the neutron reflectivity profiles acquired for the phospholipid bilayers in the absence (as presented in Figure 4) and presence of 4 μM *d*-α-synuclein.

There are many different ways to adopt the models of the unperturbed bilayers in Figure 4 to describe the data collected in the presence of protein presented in Figure 5. A key question of this study is the location of the protein in the model membranes. The fitting strategy aims to systematically obtain a physically reasonable model with a minimal number of adjustable parameters. Figure 6 shows the quality of the best fit when the protein is placed in each of the four different layers of the bilayer model, that is in the inner or outer headgroup region as well as in the inner or outer acyl chain region. These results for the four possible protein positions in the bilayer were obtained by assuming that the solvent content in one layer at a time is decreased by 10% at the same time as the SLD value of that same layer is increased to accommodate the potential presence of 10% protein. The quality of the fit is given as the error-weighted sum of squared residuals, χ^2, when applying the model to the data collected in the presence of protein. The values are plotted as a function of the assumed α-synuclein locations for the particular model used for the fitting and compared to the χ^2 obtained for the neat lipid bilayer (Figure 4). Because the SLD within each layer is assumed to be constant, the χ^2 resulting from positioning the protein in a specific layer of the bilayer model will be constant. Clearly, an improved fit is only obtained if the protein is placed in the outer headgroup region. The other three positions of the

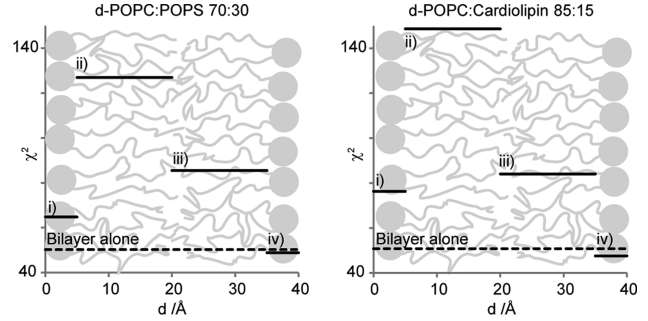

Figure 6. Weighted sum of squared residuals (χ^2) produced from data collected before and after addition of protein to surface-deposited phospholipid bilayers. To test four possible protein positions in the bilayer [(i) inner headgroup region, (ii) inner acyl chain region, (iii) outer acyl chain region, and (iv) outer headgroup region], the solvent content of one layer at a time is decreased by 10% of the total volume at the same time as the SLD value of that same layer is increased to values corresponding to the presence of 10% protein. The χ^2 from the fit when positioning the protein in a layer is plotted constant throughout the layer as the SLD in the layer is assumed to be constant. The dashed lines are χ^2 values from applying the unperturbed bilayer models (Figure 4) on data collected after addition of protein (Figure 5).

protein in the bilayer even result in impaired fits compared to the unperturbed phospholipid profiles.

The improvements in the fits due to solvent exchange in the outer headgroup region for protein are minute. For a major improvement in the fits, perturbations in the bilayer other than merely placing the protein in the outer headgroup region are required. To free space for the protein, the headgroup area in the bilayer must increase more than what is possible from just removing solvent. This can be achieved by thinning the membrane or by increasing the water content in the outer acyl chain layer. We find that thinning the outer leaflet of the bilayer together with an increased SLD value in the outer headgroup layer is not sufficient to produce good fits. However, together with an increased amount of solvent in the outer monolayer, the fitted models presented in Figure 7 and Table 2 were

dx.doi.org/10.1021/cn400066t | *ACS Chem. Neurosci.* 2013, 4, 1339−1351

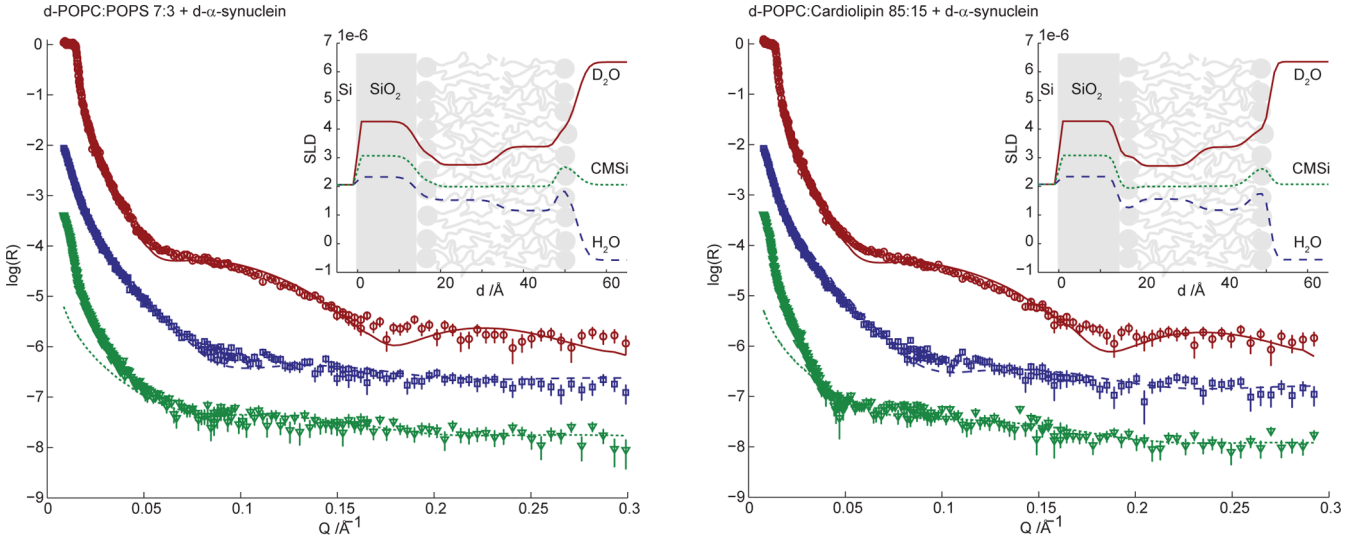

Figure 7. Neutron reflectivity (plotted as $\log_{10} R$) as a function of momentum transfer (Q) for surface-deposited 7:3 *d*-POPC/POPS (left) and 85:15 *d*-POPC/CL (right) phospholipid bilayers in the presence of 4 μM *d*-α-synuclein. The lines correspond to the fits of the multilayer models (fitting parameters in Table 2) to the experimental data. The reflectivity was measured in three solvent contrasts: D_2O (red circles), CMSi (green triangles), and H_2O (blue squares). The deviation at low Q for CMSi is instrument-dependent and was disregarded in the modeling. CMSi and H_2O profiles are offset in $\log(R)$ by −2 and −1, respectively, for the sake of clarity. The insets show the resulting SLD profiles as a function of distance from the silicon substrate.

Table 2. Parameters Obtained from Fits to Neutron Reflectivity Profiles Recorded for the Surface-Deposited 7:3 *d*-POPC/POPS, 85:15 *d*-POPC/CL, and 7:3 DOPC/DOPS Phospholipid Bilayers in the Presence of 4 μM *d*-α-Synuclein[a]

	outer acyl chain thinning (Å)	increased solvent content in outer acyl chain layer	protein volume fraction in outer headgroup layer (vol %)	lipid/protein (v/v)	lipid/protein (n/n)
7:3 *d*-POPC/POPS	1 ± 0.5	14 ± 3	12 ± 4	5.0 ± 0.4	296 ± 24
85:15 *d*-POPC/CL	1 ± 0.5	15 ± 2	14 ± 3	3.9 ± 0.3	198 ± 15
7:3 DOPC/DOPS	1 ± 0.5	5 ± 3	23 ± 5	2.3 ± 0.3	136 ± 18

[a]See Methods and Table S2 of the Supporting Information for further details of the fitting procedure and error analysis.

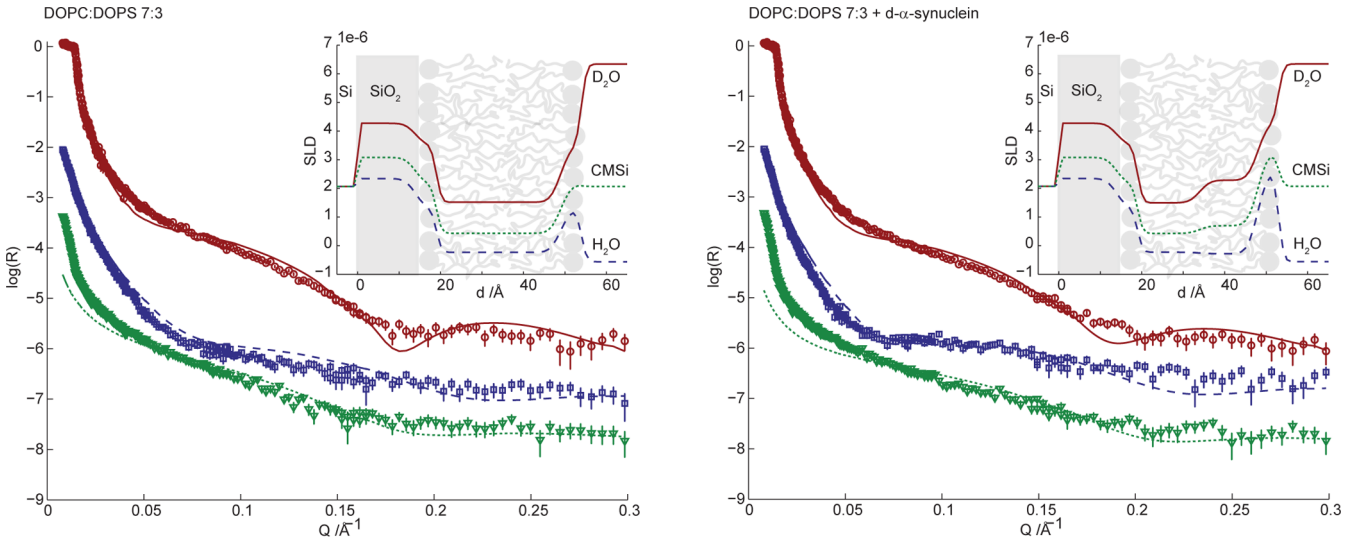

Figure 8. Neutron reflectivity (plotted as $\log_{10} R$) as a function of momentum transfer (Q) for surface-deposited 7:3 DOPC/DOPS phospholipid bilayers in the absence (left) and presence (right) of 4 μM *d*-α-synuclein. The lines correspond to the fits of the multilayer models (Tables 1 and 2) to the experimental data. The reflectivity was measured in three solvent contrasts: D_2O (red circles), CMSi (green triangles), and H_2O (blue squares). The deviation at low Q for CMSi is instrument-dependent and was disregarded in the modeling. CMSi and H_2O profiles are offset in $\log(R)$ by −2 and −1, respectively, for the sake of clarity. The insets show the resulting SLD profiles as a function of distance from the silicon substrate. An overlay of data collected before and after protein injection is presented in Figure S4 of the Supporting Information.

dx.doi.org/10.1021/cn400066t | *ACS Chem. Neurosci.* 2013, 4, 1339−1351

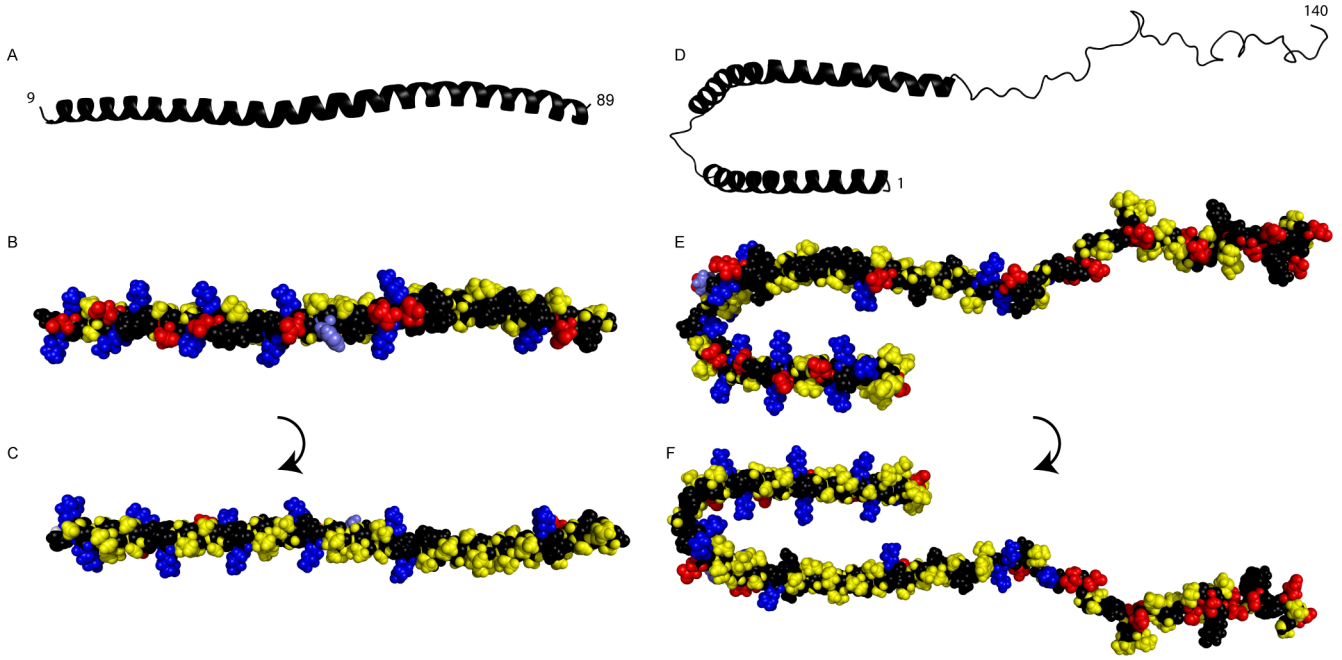

Figure 9. (A−C) Structure of an α-synuclein fragment (residues 9−89) bound to 7:3 POPC/POPS small unilamellar vesicles[30] (coordinates kindly provided by R. Langen). (D−F) Structure of α-synuclein bound to sodium dodecyl sulfate (SDS) micelles (Protein Data Bank entry 1XQ8).[53] The broken N-terminal helix in panels D−F is a result of the nature of the supporting SDS micelles and is united into one extended helix upon bilayer binding.[29,30,54] (A and D) Cartoon showing the helical N-terminus and the unstructured C-terminus. (B and E) Space filling model viewed from outside the vesicle or micelle with hydrophobic (yellow), cationic (blue), and anionic (red) residues. The titrating His50 is colored light blue for recognition. (C and F) Space filling model viewed from inside the vesicle or micelle with the same color coding.

obtained with χ^2 values of 16 and 21 for PC/PS and PC/CL bilayers, respectively. For a complete model description, see Table S2 of the Supporting Information. Many other possible scenarios to account for the bilayer perturbation upon protein adsorption were modeled, for example, increasing the solvent content throughout the bilayer, changing the thickness of the different layers, and placing the protein outside the bilayer. None of these scenarios improved the fits as much as applying the models presented in Figure 7 and Table 2.

The fits in Figure 7 were obtained by keeping all parameters from the bilayer fits constant except for the thickness and solvent content of the acyl chain layer in the outer leaflet, and the SLD in the outer headgroup layer. The acyl chain layer thickness was first fit by comparing the model with the experimental data followed by simultaneous modeling of the solvent content in the acyl chain slab layer and headgroup SLD using least-squares minimization. The solvent content in the outer headgroup layer was matched to preserve the stoichiometry between headgroups and acyl chains. The changes in the models for the outer monolayers compared to the neat bilayers are listed in Table 2 together with the corresponding protein concentrations given from the fitted headgroup SLD (Table S2 of the Supporting Information). The reported protein occupancies should be taken as maximal values because they are calculated from a model where the protein is completely contained within the headgroup layer of the bilayer. The fits to data obtained for both 7:3 *d*-POPC/POPS and 85:15 *d*-POPC/CL bilayers in the presence of monomeric *d*-α-synuclein resulted in very similar perturbations of the bilayers and amounts of adsorbed protein.

Increased Area per Phospholipid Headgroup. It has been suggested that the insertion of α-synuclein into the membrane can be facilitated by increasing the available area per phospholipid headgroup in the interface.[50] An increase in lipid headgroup area implies greater exposure of the hydrocarbon region in the bilayer.[51] To investigate this aspect, an additional experiment was conducted using a 7:3 DOPC/DOPS bilayer. The phase behavior, headgroups, and charge density are similar to that of the POPC/POPS system, but the area per headgroup is slightly larger because of the more bulky acyl chainss of DOPC as both chains are unsaturated.[52] By using a protonated bilayer, the contrast against the perdeuterated protein is altered compared to those of previously studied systems (Figure S2 of the Supporting Information). Figure 8 shows the neutron reflectivity profiles recorded for a supported 7:3 DOPC/DOPS bilayer in the absence (left panel) and presence (right panel) of *d*-α-synuclein. The fitting procedure is the same as in previous experiments but with a new bilayer composition. The last row of Table 1 presents the fitted model parameters. The deposition coverage is lower compared to those of previous systems, and the fit is not as good; however, the qualitative changes upon protein adsorption are similar. The results from fitting the model to the data recorded after adsorption of protein (Table 2) to the bilayer show that protein occupies 23% of the outer headgroup layer volume. This should be compared to protein volume fractions of 12 and 14% in the headgroup region of *d*-POPC/POPS and *d*-POPC/CL bilayers, respectively. In agreement with these results, QCM-D of association of α-synuclein with DOPC/DOPS bilayers indicates a 27% increase in protein film thickness and very similar shear and viscosity (Figure S3 of the Supporting Information) compared to those of the POPC/DOPS bilayer presented in Figure 3.

DISCUSSION

In this study, we define the molecular determinants for adsorption of monomeric α-synuclein to planar model

membranes, determine the position of the protein, and detect structural changes in the model membranes. This information is obtained from the combination of two complementary surface-sensitive techniques, QCM-D and NR, and from using well-defined model systems of monomeric protein, bilayers containing one or two types of lipids, and different solution conditions. Our data clearly demonstrate specificity in α-synuclein−membrane interaction in terms of membrane composition. The molecular origin of this interaction most likely lies in the uneven distribution of charged and nonpolar residues in α-synuclein (Figure 9) and in the mixed lipid bilayer.

Association Is Governed by Electrostatic Interactions between the Protein and Bilayer. Because α-synuclein has a net charge of −7 at pH 5.5, one expects an overall electrostatic repulsion between the protein and an anionic bilayer. However, both QCM-D and NR measurements reveal that α-synuclein adsorbs to bilayers that contain anionic lipids, in accordance with other studies,[50,55−57] while there is no adsorption to zwitterionic PC bilayers. The high affinity of α-synuclein for anionic lipids has been reconciled with the polarized nature of the protein.[50] The N-terminal half is positively charged (+2 at pH 7 and +4 at pH 5.5), and the C-terminal half is negatively charged (−11 at both pH values). A series of repeats in the N-terminal half are arranged so that, if this part folds into an α-helix upon membrane association, the helix has one polar (Figure 9B) and one hydrophobic (Figure 9C) side with lysine residues flanking the borders between them.

The anionic lipids PS and CL are structurally very different. Still, both the QCM-D and NR experiments show that the association of α-synuclein is similar for bilayers that contain either of these lipids as long as the lipid composition is chosen so that bilayer charge density is the same. The carboxyl group in PS is expected to be fully deprotonated at the pH used in this study.[58] Recent pH titration and calorimetry studies of the dispersed sodium salt of synthetic CL, which is used in this study, show that both phosphates in the CL headgroup are deprotonated above pH 3.[59] This is in contrast to previous reports of the titration of CL extracts from beef heart and *Escherichia coli*, which reported that the CL headgroup is partially protonated around physiological pH.[60]

Protein Film Compactness Depends on pH and Salt Concentration. The dissipation and overtone-dependent frequency shift contain information about the viscoelastic properties of the film. The large dissipation and strong dependence of the frequency shift on the overtones imply that the film is viscous and/or that it extends into solution giving rise to higher shear tension. The applied viscoelastic modeling of the observed shifts (Figures 1 and 2) supports the view of the C-terminal part as extending out from the bilayer as a polymer brush. The thickness of the protein film is between 0 and 8 nm (Figure 2) depending on the bilayer and solution composition. This is compatible with an unfolded C-terminus of membrane-associated α-synuclein. The distance between the C-terminus and Thr92 at the end of the second helix is 8 nm in the micelle-bound structure presented in Figure 9. Our QCM-D results are also compatible with the low protein density region extending 6.3 nm from the 1:1 PC/PA bilayer at 110 mM salt and pH 7.4 modeled by Pfefferkorn et al.[28] as the increases in both salt concentration and pH make the protein film thinner. At pH 5.5 and a low salt concentration, the C-terminal part of the protein appears to be extended in a polymer brush-like conformation.

The increased shear modulus and viscosity of the extending protein film suggest that the film is not only thicker but also denser at low salt concentrations and pH values. This finding indicates that the protein film thickness is dependent on, and might be a consequence of, how much protein is associated with the bilayer. The repulsion between the extending C-terminal parts likely imposes a correlation between how much α-synuclein is associated and how far the protein extends into the bulk. This is in accordance with the previously reported increase in the helical content of α-synuclein at low salt concentrations in the presence of anionic lipids.[57,61] At low pH, the N-terminus and the histidine at position 50 are likely protonated, which decreases the level of repulsion between the protein and the bilayer as well as between the proteins. This is expected to allow for a more dense packing of the protein at the bilayer and thus a more extended protein film. The striking similarity between the results for PS- and CL-containing bilayers implicates a dominating contribution from balancing electrostatic interactions between protein and lipids. However, electrostatic interactions are long-range and involve multiple contributions from phospholipids, lysines, negative residues, and ions and are hard to fully predict.

While the QCM-D experiments capture the properties of the extending protein outside of the bilayer, it measures only the total amount on the surface and therefore cannot determine if lipids are exchanged for protein in the bilayer. The NR experiments are therefore complementary to the QCM-D experiments and capture the composition of the bilayer, the location of the protein in the bilayer, and how the structure of the bilayer is affected.

α-Synuclein Is Mainly Embedded in the Outer Headgroup Area. The NR data show very similar modes of adsorption to the CL- and PS-containing bilayers. A recent NR study of adsorption of α-synuclein to 1:1 PC/PA tethered bilayers at pH 7 proposed a penetration depth of 9−14 Å in the outer leaflet of the bilayer with a substantial portion of the protein outside of the bilayer.[28] In that study, a continuous model with more degrees of freedom was used, as compared to the slab model used here. The motivation for our approach is to limit the number of degrees of freedom by using as few adjustable parameters as possible. Furthermore, data from three contrasts were recorded and used in the analysis for each type of bilayer/protein system. Figure 3 and Figure S2 of the Supporting Information illustrate the isotope composition for all studied bilayers. The bilayers were successfully modeled as being symmetric, using three independent variables and the background intensities. Upon protein association, as few changes as possible were made to the bilayer model, conserving stoichiometric restrictions to improve the fits to the same level as the bilayer fits. This conservative application of Occam's razor leads to a model that does not try to capture all structural aspects but captures the major aspects as theoretically robustly as possible. We found that tentatively placing the protein in different locations and comparing the resulting fits to the data is a fruitful approach that clearly discards models in which the protein is fully buried among the acyl chains or in the inner headgroup layer close to the support. Embedding the protein in the outer headgroup area stands out as the only model that can describe the experimental data, supporting the idea that the protein is penetrating into the membrane, but the models suggest that the penetration of the protein is shallow. In addition to the protein present in the headgroup layer, Pfefferkorn et al.[28] found a low protein density in the outer

acyl chain layer. Here, such addition resulted in impaired fits, but instead, we found an improved fit with an increase in the water content in the outer leaflet. To be able to distinguish protein from water in the bilayer, one requires several isotopic compositions of the bilayer, protein, and solvent, and this was achieved by measuring at three contrasts, by using a lipid mixture producing an intermediate SLD, and by using a deuterated protein with a high SLD. Our data together with the slab model do not provide information about lateral structure, and we cannot distinguish, for example, clustering of anionic lipids in the vicinity of the adsorbed proteins as previously has been shown by others.[56,62]

Protein Adsorption Leads to Thinning and Increased Water Content in the Lipid Membrane. A minor thinning of the bilayer to free space for the protein in the headgroup layer was needed in the modeling, which is also consistent with the previous NR study for another lipid composition and pH.[28] However, the thinning does not free enough space for the protein to be located between the outer phospholipid headgroups. A perturbed acyl chain packing with increased water content in the acyl chain layer is needed in addition to the thinning of the bilayer to observe a good fit while preserving stoichiometric relations. Exchanging the neutral phospholipid component from POPC to DOPC in the supported bilayer results in an increased level of α-synuclein association with less water in the acyl chain layer (Table 2). The more perturbed packing induced by the extra unsaturation in the acyl chains thus favors protein association and avoids the increased amount of water in the hydrophobic acyl chain region. It is interesting to correlate this finding with the fact that long chain superunsaturated fatty acids, such as docosahexanoic, eicosapentaoic, and arachidonic acid with six, five, and four double bonds, respectively, are highly over-represented in brain and neuronal membranes.[63]

Mutual Disruption. Interaction between amyloid proteins and membranes may result in mutually disruptive structural perturbations. Membrane surfaces may alter the rate of conversion of amyloid-forming proteins into toxic aggregates, and amyloidogenic proteins. Such aggregates may, in turn, pick up membrane lipids or compromise the structural integrity of the membranes. In many amyloid diseases, oligomeric species rather than mature amyloid fibrils seem to be responsible for cytotoxicity. In addition, the toxicity of amyloid proteins seems to correlate with their interactions with cell membranes.[64] This finding has been inferred to arise from the amyloid protein affecting the membrane structure and permeability, but it may also be the membrane affecting the protein self-assembly. In the case of α-synuclein, an amyloid pore hypothesis has been around for some time. It assumes that annular oligomeric species form protein channels or pores, through lipid bilayers, which increase permeability and lead to toxicity. In part, the increased permeability seen could be considered to be consistent with the thinning of the lipid bilayer observed here and the increased amount of solvent in the outer acyl chain region, although there are conflicting reports about monomer-induced leakage.[30,61,65] However, pore formation is not consistent with the present observation of recombinant α-synuclein in deposited mixed bilayers as the protein is present in only the interfacial region of the bilayer, as demonstrated via NR. In a third scenario, the critical event may be a co-aggregation process, in which membrane lipids associate with the aggregating protein and associate on pathway and in final protein aggregate structures.

CONCLUDING REMARKS

We have shown selective adsorption of α-synuclein to anionic supported lipid bilayers with the biologically relevant membrane lipids, PC, PS, and CL. Independent of the anionic headgroup identity, the main part of the protein is positioned in the headgroup region of the bilayer and does not penetrate deeply into or across the hydrophobic acyl chain region. Furthermore, the position in the headgroup region leads to a nearly identical increase in the solvent content of the outer acyl chain region, independent of the identity of the anionic headgroup. The C-terminal extension outside of the bilayer is tuned by electrostatic interactions. The adsorbed amount and the properties of the adsorbed protein layer depend on electrostatic shielding and protein charge as well as headgroup separation.

METHODS

Materials. Partially deuterated and hydrogenated lipids were purchased in lyophilized form from Avanti Polar Lipids (Alabaster, AL): 1-palmitoyl(*d*-31)-2-oleoyl-*sn*-glycero-3-phosphocholine (*d*-POPC), 1-palmitoyl-2-oleoyl-*sn*-glycero-3-phosphocholine (POPC), 1,2-dioleoyl-*sn*-glycero-3-phosphocholine (DOPC), 1-palmitoyl-2-oleoyl-*sn*-glycero-3-phospho-L-serine (POPS), 1,2-dioleoyl-*sn*-glycero-3-phospho-L-serine (DOPS), and 1′,3′-bis(1,2-dioleoyl-*sn*-glycero-3-phospho)-*sn*-glycerol (CL). All chemicals were of analytical grade, and the water used was ultrapure (<18.2 MΩ cm at 25 °C, Milli-Q grade). Human α-synuclein, which was used for the QCM-D measurements, was expressed in *E. coli* from the aS-pT7-7 plasmid (kindly provided by H. Lashuel) and purified using heat treatment, ion exchange, and gel filtration chromatography as previously described.[48] For perdeuteration of α-synuclein, the resistance marker of aS-pT7-7 was changed by *in vitro* transposition from ampicillin to kanamycin using the (EZ-Tn5) <KAN-2> Insertion Kit from Epicenter Biotechnologies. The modified plasmid was then transformed into BL21(DE3) cells. A high-cell density fed-batch culture using d_8-glycerol (Euriso-top) as a carbon source was conducted in the joint ILL-EMBL Deuteration Laboratory with a computer-controlled temperature of 30 °C, a pD of 6.9, and a pO_2 of 30% saturation.[66] α-Synuclein expression was induced with 0.2 mM isopropyl thiogalactopyranoside and the deuterated protein purified as described previously.[48] The molecular mass for *d*-α-synuclein was determined by mass spectrometry to be 15209 Da in H_2O. If all labile deuterons in α-synuclein are assumed to be exchanged, the extent of deuteration is calculated to be 97%.

Protein Sample Preparation. α-Synuclein, purified as stated above, was transferred to the desired buffer solution, 10 mM MES (pH 5.5) with or without 150 mM NaCl and 10 mM HEPES (pH 7.0), by fast protein liquid chromatography using a size exclusion column (Superdex 75, GE Healthcare). Only the central fraction of the monomer peak was collected to ensure a monomeric sample. The protein concentration was determined by integration of the absorbance at 280 nm for the collected fractions using an extinction coefficient of 5960 M^{-1} cm^{-1}. For QCM-D experiments, the monomer solution was diluted to 4 μM with the experimental buffer solution and kept on ice until the solution was injected (<5 h). For neutron reflectometry measurements, which for all recorded data shown used *d*-α-synuclein, the monomer solution was freeze-dried, stored in a freezer, dissolved to a concentration of 4 μM in buffer, and diluted with water to restore the ionic strength to the pre-freeze-drying values. The redissolved monomeric protein after freeze-drying was validated still to be monomeric by size exclusion chromatography (Figure S5 of the Supporting Information). The solutions were prepared immediately prior to the start of the experiment. As shown in Figure S6 of the Supporting Information, identical reflectometry profiles are recorded before and after a full experiment in D_2O. This suggests that no aggregation occurs during the time of the experiment.

The protein concentration was 4 μM in all experiments and could not be increased in the QCM-D experiments as the response is also

sensitive to changes in solvent viscosity. However, when 8 μM protein was re-injected after completion of the NR measurement at 4 μM, identical reflectivity profiles were collected in D_2O and H_2O (Figure S7 of the Supporting Information), implying that 4 μM protein is enough for saturation of the supported bilayer.

Bilayer Formation. Bilayers were deposited from sonicated vesicles by spontaneous vesicle fusion and spreading on the supporting surface. Lipids were mixed in a 9:1 (v/v) chloroform/methanol solution, deposited as a thin film on glass under a slow flow of nitrogen gas, and then dried under vacuum overnight. Prior to the experiments, the lipid films were hydrated with H_2O for zwitterionic lipids (DOPC/POPC) or with 200 mM NaCl for lipid mixtures containing anionic lipids (DOPC/POPC and DOPS/POPS or CL). The increased anionic strength used with the anionic lipid mixtures is necessary for screening of silica−vesicle and vesicle−vesicle electrostatic repulsions to promote vesicle fusion and spreading into a proper bilayer. The final phospholipid concentration used for vesicle deposition was 0.5 mg/mL. The lipid dispersions were probe sonicated until they appeared to be clear and then centrifuged for 2 min (>10000g) to remove trace particles from the probe. The vesicle dispersion was passed through the sample cell for 10 min, which was shown to be sufficient time for a complete bilayer to form. The vesicular dispersion was then replaced with H_2O in the case of a noncharged bilayer and first 200 mM NaCl and then H_2O in the case of anionic lipid bilayers. The bilayers were equilibrated in the buffer solution before characterization and protein injection.

QCM-D. The QCM-D instrument was a Q-sense E4 instrument from Q-sense (Gothenburg, Sweden). The measuring cells were thermostated at 25 °C. The quartz crystals had a fundamental frequency of 4.95 MHz and were covered by a thin gold surface coated with 50 nm SiO_2 (QSX 303, Q-sense). The coated crystals were cleaned and stored for a minimum of 1 h in a 2% sodium dodecyl sulfate solution before being used. After being rinsed in deionized water followed by ethanol, the crystals were dried with nitrogen and then treated under a reduced air pressure (0.02 mbar) in a plasma cleaner (model PDC-3XG, Harrick Scientific Corp., Pleasantville, NY) for 5 min. After the crystals had been mounted in the instrument, they were equilibrated in H_2O until a steady response in frequency and dissipation had been realized. A peristaltic pump (Ismatec IPC-N4) controlled the flow through the four parallel measuring cells. The flow rates used during bilayer deposition and protein injection were 100 and 50 μL/min, respectively.

QCM-D Modeling. All data treatment and modeling were conducted using Qtools version 3.0.17.560 (Biolin scientific AB, Gothenburg, Sweden). The bilayer film before addition of protein was modeled as a dense film using a Sauerbrey representation. According to the Sauerbrey equation, the frequency shift in QCM-D is proportional to the acoustic mass of dense layers:[67]

$$\Delta m = \frac{C}{n}\Delta F$$

where ΔF is the frequency shift, C is a crystal specific constant of 17.7 ng Hz^{-1} cm^{-2} for the used crystals, and n is the overtone number. Modeling of the viscoelastic protein film was done using a Voight representation keeping the fluid density (1000 kg/m^3), fluid viscosity (0.001 kg/ms), and layer density (1000 kg/m^3) fixed. The viscosity, shear modulus, and thickness of the film were globally fit to frequency and dissipation for overtone numbers 5, 7, and 9.

Neutron Reflectometry. NR measurements were performed using the SURF reflectometer at ISIS (Oxford, U.K.), D17 at ILL (Grenoble, France), and the Liquids Reflectometer (LR) at SNS/ORNL (Oak Ridge, TN). Presented data were collected using the LR at SNS/ORNL. Single-crystal silicon blocks (5 cm × 5 cm × 1 cm) with the side facing the solution being polished (Siltronix, France) to a roughness of 2−3 Å were used as substrates for NR measurement. The spontaneously formed silicon oxide layer, which after being polished had a thickness of 14 Å, was characterized in three different solvent contrasts: D_2O, 38:62 (v/v) D_2O/H_2O contrast matched to silicon (CMSi), and H_2O. The substrates were cleaned at 80 °C for 15 min using a dilute Piranha solution composed of water, sulfuric acid (98%), and hydrogen peroxide (27.5%) in a 5:4:1 volume ratio. The substrates were either vertically (D17-ILL) or horizontally (SURF-ISIS, LR-SNS) mounted, with the polished surface facing downward to a 5 mL Teflon flow cell with magnetic stirring.[68] The measuring cell was held at 25 °C. All liquid exchange was achieved using a high-performance liquid chromatography pump and a minimum of 20 mL of liquid, i.e., 4 times the measuring cell volume. All measurements were performed in the three solvent contrasts mentioned above. To preserve the protonation state of α-synuclein in all contrasts, pH and pH* were controlled and corrected in H_2O- and D_2O-based buffers, respectively, without correcting pH* to pD.[69−71]

Neutron Reflectometry Modeling. The results from neutron reflectivity (NR) are presented as reflectivity profiles with normalized intensity as a function of the momentum transfer vector, which in specular reflection equals the scattering vector Q. Q then depends on both the neutron wavelength, λ, and the angle of incidence, θ, according to

$$Q = \frac{4\pi}{\lambda}\sin\theta$$

A brief synopsis on NR methodology and analysis is given in an earlier review on related applications.[72] The reflectivity profiles were analyzed using RasCal (version 1.1.2, A. Hughes, ISIS Spallation Neutron Source, Rutherford Appleton Laboratory),[73] which allows multicontrast modeling of Abeles layer models to the surface structure. In this approach, the scattering length density (SLD) profile is described as a series of defined layers. Each layer is characterized by three parameters: SLD, thickness, and roughness. The SLD of each layer was further separated into the SLD contributions from the layer components and solvent volume fraction, based on the SLD of the pure substances. Each layer was therefore characterized by a total of four parameters, which are partially dependent.

SLDs for the lipids were calculated from atomic composition, c_i, with coherent scattering lengths, b_c, and molecular volumes, V_m, from molecular dynamics simulations[74,75] according to

$$\mathrm{SLD} = \frac{\sum_{i=1}^{n} b_{c_i}}{V_m}$$

To the best of our knowledge, there are no available data from measurements or simulations on the headgroup volume of CL, and we therefore used the molecular density of PG[76,77] because CL structurally consists of two linked PG molecules. The calculated lipid SLD values were allowed to vary up to 10% during modeling. For all experimental data, the fits were found to improve if the lipid SLD values were decreased by 10% compared to those calculated, corresponding to 10% larger molecular volumes. The SLD of d-α-synuclein was calculated on the basis of its atomic composition using a typical protein density for hydrogenated protein of 1.37 g/cm^3.[78] The perdeuterated protein SLD values were calculated to 6.48, 6.99, and 7.84 in H_2O, CMSi, and D_2O, respectively, taking exchanging protons into account. The average of these three calculated values was used when translating the fitted SLD in a layer to protein volume occupancy, because the SLD of a layer (excluding contained solvent) was set to be the same in all contrasts to allow simultaneous fitting by least-squares minimization. Recalculating the contrast-dependent SLD for the headgroup−protein layer from the modeled protein occupancy showed a deviation in SLD of 0.1×10^{-6} Å^{-2} in D_2O and -0.1×10^{-6} Å^{-2} in H_2O. The fit resulted in a deviation, χ^2, within 0.3. The thickness of each layer was fit in steps of 1 Å without using least-squares minimization, because of the sensitivity to scaling in the Q direction, which is not captured well in error minimization in the logarithmic reflectivity [log(R)] direction. A 1 Å reduction in outer acyl chain thickness upon protein addition clearly improved the fits in the Q direction, while a larger reduction resulted in impaired fits. The resolution in the measurement in combination with our strict fitting criteria did not allow for higher resolution in the modeling of thicknesses. The solvent volume fraction in the acyl chain layer was fit by error-weighted least-squares minimization in an iterative way, while

adjusting the solvent volume fraction in the headgroup layer to conserve the head-to-tail stoichiometry in the phospholipids. Fitting of the multilayer model was done globally to experimental data for all contrasts. The Q ranges used in the fitting procedure was 0.03−0.3 for D_2O and 0.05−0.3 for CMSi and H_2O due to instrument-related deviation at low Q values.

■ ASSOCIATED CONTENT

Supporting Information

Supporting figures and tables. This material is available free of charge via the Internet at http://pubs.acs.org.

■ AUTHOR INFORMATION

Funding

This work was supported by the Swedish Research Council and its Linneaus programme OMM (E.H., E.S., S.L., and T.N.), Lund University Science Faculty (E.S., T.N., S.L.), The Swedish Foundation for Strategic Research (E.S.), the Crafoord Foundation (S.L.), the Royal Physiographic Society (E.H.), MultiPark (E.H., M.G., and P.B.), ERC Advanced Award 269064-'PRISTINE-PD' (P.B.), EPSRC support (EP/C015452/1) to V. T. Forsyth (Keele University, Staffordshire, U.K.) for the creation of the Deuteration Laboratory within ILL's Life Science group, and the EU under Contract RII3-CT-2003-505925 (M.H. and V.T.F.). Work at ORNL was performed under DOE contract DE-AC05-00OR22725.

Notes

The authors declare no competing financial interest.

■ ACKNOWLEDGMENTS

We thank ILL, ISIS, and SNS for allocation of beam time and Candice Halbert and Jim Browning for assistance during the SNS experiment as well as Arwel Hughes and Luke Clifton during the ISIS experiments. We also thank Robert K. Thomas for valuable discussions concerning the interpretation and modeling of neutron data and Anna Stradner for valuable comments on the manuscript.

■ REFERENCES

(1) Schapira, A. H. (2009) Neurobiology and treatment of Parkinson's disease. *Trends Pharmacol. Sci. 30*, 41−47.

(2) Graham, J. M., and Sagar, H. J. (1999) A data-driven approach to the study of heterogeneity in idiopathic Parkinson's disease: Identification of three distinct subtypes. *Mov. Disord. 14*, 10−20.

(3) Polymeropoulos, M. H., Lavedan, C., Leroy, E., Ide, S. E., Dehejia, A., Dutra, A., Pike, B., Root, H., Rubenstein, J., Boyer, R., Stenroos, E. S., Chandrasekharappa, S., Athanassiadou, A., Papapetropoulos, T., Johnson, W. G., Lazzarini, A. M., Duvoisin, R. C., Di Iorio, G., Golbe, L. I., and Nussbaum, R. L. (1997) Mutation in the α-synuclein gene identified in families with Parkinson's disease. *Science 276*, 2045−2047.

(4) Kruger, R., Kuhn, W., Muller, T., Woitalla, D., Graeber, M., Kosel, S., Przuntek, H., Epplen, J. T., Schols, L., and Riess, O. (1998) Ala30Pro mutation in the gene encoding α-synuclein in Parkinson's disease. *Nat. Genet. 18*, 106−108.

(5) Zarranz, J. J., Alegre, J., Gomez-Esteban, J. C., Lezcano, E., Ros, R., Ampuero, I., Vidal, L., Hoenicka, J., Rodriguez, O., Atares, B., Llorens, V., Gomez Tortosa, E., del Ser, T., Munoz, D. G., and de Yebenes, J. G. (2004) The new mutation, E46K, of α-synuclein causes Parkinson and Lewy body dementia. *Ann. Neurol. 55*, 164−173.

(6) Chartier-Harlin, M. C., Kachergus, J., Roumier, C., Mouroux, V., Douay, X., Lincoln, S., Levecque, C., Larvor, L., Andrieux, J., Hulihan, M., Waucquier, N., Defebvre, L., Amouyel, P., Farrer, M., and Destee, A. (2004) α-Synuclein locus duplication as a cause of familial Parkinson's disease. *Lancet 364*, 1167−1169.

(7) Singleton, A. B., Farrer, M., Johnson, J., Singleton, A., Hague, S., Kachergus, J., Hulihan, M., Peuralinna, T., Dutra, A., Nussbaum, R., Lincoln, S., Crawley, A., Hanson, M., Maraganore, D., Adler, C., Cookson, M. R., Muenter, M., Baptista, M., Miller, D., Blancato, J., Hardy, J., and Gwinn-Hardy, K. (2003) α-Synuclein locus triplication causes Parkinson's disease. *Science 302*, 841.

(8) Halliday, G. M., Ophof, A., Broe, M., Jensen, P. H., Kettle, E., Fedorow, H., Cartwright, M. I., Griffiths, F. M., Shepherd, C. E., and Double, K. L. (2005) α-Synuclein redistributes to neuromelanin lipid in the substantia nigra early in Parkinson's disease. *Brain 128*, 2654−2664.

(9) Halliday, G. M., Holton, J. L., Revesz, T., and Dickson, D. W. (2011) Neuropathology underlying clinical variability in patients with synucleinopathies. *Acta Neuropathol. 122*, 187−204.

(10) Winner, B., Jappelli, R., Maji, S. K., Desplats, P. A., Boyer, L., Aigner, S., Hetzer, C., Loher, T., Vilar, M., Campioni, S., Tzitzilonis, C., Soragni, A., Jessberger, S., Mira, H., Consiglio, A., Pham, E., Masliah, E., Gage, F. H., and Riek, R. (2011) In vivo demonstration that α-synuclein oligomers are toxic. *Proc. Natl. Acad. Sci. U.S.A. 108*, 4194−4199.

(11) Wakabayashi, K., Tanji, K., Mori, F., and Takahashi, H. (2007) The Lewy body in Parkinson's disease: Molecules implicated in the formation and degradation of α-synuclein aggregates. *Neuropathology 27*, 494−506.

(12) Harrower, T. P., Michell, A. W., and Barker, R. A. (2005) Lewy bodies in Parkinson's disease: Protectors or perpetrators? *Exp. Neurol. 195*, 1−6.

(13) Bartels, T., Choi, J. G., and Selkoe, D. J. (2011) α-Synuclein occurs physiologically as a helically folded tetramer that resists aggregation. *Nature 477*, 107−110.

(14) Fauvet, B., Fares, M. B., Samuel, F., Dikiy, I., Tandon, A., Eliezer, D., and Lashuel, H. A. (2012) Characterization of semisynthetic and naturally Nα-acetylated α-synuclein in vitro and in intact cells: Implications for aggregation and cellular properties of α-synuclein. *J. Biol. Chem. 287*, 28243−28262.

(15) Davidson, W. S., Jonas, A., Clayton, D. F., and George, J. M. (1998) Stabilization of α-synuclein secondary structure upon binding to synthetic membranes. *J. Biol. Chem. 273*, 9443−9449.

(16) Conway, K. A., Harper, J. D., and Lansbury, P. T. (1998) Accelerated in vitro fibril formation by a mutant α-synuclein linked to early-onset Parkinson disease. *Nat. Med. 4*, 1318−1320.

(17) Conway, K. A., Harper, J. D., and Lansbury, P. T., Jr. (2000) Fibrils formed in vitro from α-synuclein and two mutant forms linked to Parkinson's disease are typical amyloid. *Biochemistry 39*, 2552−2563.

(18) Murphy, D. D., Rueter, S. M., Trojanowski, J. Q., and Lee, V. M. (2000) Synucleins are developmentally expressed, and α-synuclein regulates the size of the presynaptic vesicular pool in primary hippocampal neurons. *J. Neurosci. 20*, 3214−3220.

(19) Bussell, R., Jr., and Eliezer, D. (2003) A structural and functional role for 11-mer repeats in α-synuclein and other exchangeable lipid binding proteins. *J. Mol. Biol. 329*, 763−778.

(20) Eliezer, D., Kutluay, E., Bussell, R., Jr., and Browne, G. (2001) Conformational properties of α-synuclein in its free and lipid-associated states. *J. Mol. Biol. 307*, 1061−1073.

(21) el-Agnaf, O. M., and Irvine, G. B. (2002) Aggregation and neurotoxicity of α-synuclein and related peptides. *Biochem. Soc. Trans. 30*, 559−565.

(22) Bussell, R., Jr., and Eliezer, D. (2004) Effects of Parkinson's disease-linked mutations on the structure of lipid-associated α-synuclein. *Biochemistry 43*, 4810−4818.

(23) Bodner, C. R., Maltsev, A. S., Dobson, C. M., and Bax, A. (2010) Differential phospholipid binding of α-synuclein variants implicated in Parkinson's disease revealed by solution NMR spectroscopy. *Biochemistry 49*, 862−871.

(24) Dunning, C. J., Reyes, J. F., Steiner, J. A., and Brundin, P. (2012) Can Parkinson's disease pathology be propagated from one neuron to another? *Prog. Neurobiol. 97*, 205−219.

(25) Danzer, K. M., Kranich, L. R., Ruf, W. P., Cagsal-Getkin, O., Winslow, A. R., Zhu, L., Vanderburg, C. R., and McLean, P. J. (2012) Exosomal cell-to-cell transmission of α-synuclein oligomers. *Mol. Neurodegener. 7*, 42.
(26) Bellingham, S. A., Guo, B. B., Coleman, B. M., and Hill, A. F. (2012) Exosomes: Vehicles for the transfer of toxic proteins associated with neurodegenerative diseases? *Front. Physiol. 3*, 124.
(27) Alvarez-Erviti, L., Seow, Y., Schapira, A. H., Gardiner, C., Sargent, I. L., Wood, M. J., and Cooper, J. M. (2011) Lysosomal dysfunction increases exosome-mediated α-synuclein release and transmission. *Neurobiol. Dis. 42*, 360−367.
(28) Pfefferkorn, C. M., Heinrich, F., Sodt, A. J., Maltsev, A. S., Pastor, R. W., and Lee, J. C. (2012) Depth of α-synuclein in a bilayer determined by fluorescence, neutron reflectometry, and computation. *Biophys. J. 102*, 613−621.
(29) Jao, C. C., Der-Sarkissian, A., Chen, J., and Langen, R. (2004) Structure of membrane-bound α-synuclein studied by site-directed spin labeling. *Proc. Natl. Acad. Sci. U.S.A. 101*, 8331−8336.
(30) Jao, C. C., Hegde, B. G., Chen, J., Haworth, I. S., and Langen, R. (2008) Structure of membrane-bound α-synuclein from site-directed spin labeling and computational refinement. *Proc. Natl. Acad. Sci. U.S.A. 105*, 19666−19671.
(31) Devi, L., Raghavendran, V., Prabhu, B. M., Avadhani, N. G., and Anandatheerthavarada, H. K. (2008) Mitochondrial import and accumulation of α-synuclein impair complex I in human dopaminergic neuronal cultures and Parkinson disease brain. *J. Biol. Chem. 283*, 9089−9100.
(32) Rothman, J. E., and Lenard, J. (1977) Membrane asymmetry. *Science 195*, 743−753.
(33) Buckland, A. G., and Wilton, D. C. (2000) Anionic phospholipids, interfacial binding and the regulation of cell functions. *Biochim. Biophys. Acta 1483*, 199−216.
(34) Vance, J. E. (2008) Phosphatidylserine and phosphatidylethanolamine in mammalian cells: Two metabolically related aminophospholipids. *J. Lipid Res. 49*, 1377−1387.
(35) Zigoneanu, I. G., Yang, Y. J., Krois, A. S., Haque, E., and Pielak, G. J. (2012) Interaction of α-synuclein with vesicles that mimic mitochondrial membranes. *Biochim. Biophys. Acta 1818*, 512−519.
(36) Cho, N. J., Frank, C. W., Kasemo, B., and Hook, F. (2010) Quartz crystal microbalance with dissipation monitoring of supported lipid bilayers on various substrates. *Nat. Protoc. 5*, 1096−1106.
(37) Glasmastar, K., Larsson, C., Hook, F., and Kasemo, B. (2002) Protein adsorption on supported phospholipid bilayers. *J. Colloid Interface Sci. 246*, 40−47.
(38) Hook, F., Kasemo, B., Nylander, T., Fant, C., Sott, K., and Elwing, H. (2001) Variations in coupled water, viscoelastic properties, and film thickness of a Mefp-1 protein film during adsorption and cross-linking: A quartz crystal microbalance with dissipation monitoring, ellipsometry, and surface plasmon resonance study. *Anal. Chem. 73*, 5796−5804.
(39) Furman, O., Usenko, S., and Lau, B. L. (2013) Relative importance of the humic and fulvic fractions of natural organic matter in the aggregation and deposition of silver nanoparticles. *Environ. Sci. Technol. 47*, 1349−1356.
(40) Vandoolaeghe, P., Rennie, A. R., Campbell, R. A., Thomas, R. K., Höök, F., Fragneto, G., Tiberg, F., and Nylander, T. (2008) Adsorption of cubic liquid crystalline nanoparticles on model membranes. *Soft Matter 4*, 2267.
(41) Voinova, M. V., Rodahl, M., Jonson, M., and Kasemo, B. (1999) Viscoelastic Acoustic Response of Layered Polymer Films at Fluid-Solid Interfaces: Continuum Mechanics Approach. *Phys. Scr. 59*, 391−396.
(42) Scott, C. C., and Gruenberg, J. (2011) Ion flux and the function of endosomes and lysosomes: pH is just the start: The flux of ions across endosomal membranes influences endosome function not only through regulation of the luminal pH. *BioEssays 33*, 103−110.
(43) Cole, N. B., Dieuliis, D., Leo, P., Mitchell, D. C., and Nussbaum, R. L. (2008) Mitochondrial translocation of α-synuclein is promoted by intracellular acidification. *Exp. Cell Res. 314*, 2076−2089.
(44) Orski, S. V., Kundu, S., Gross, R., and Beers, K. L. (2013) Design and implementation of two-dimensional polymer adsorption models: Evaluating the stability of *Candida antarctica* lipase B/solid-support interfaces by QCM-D. *Biomacromolecules 14*, 377−386.
(45) Luna, E. J., and McConnell, H. M. (1977) Lateral phase separations in binary mixtures of phospholipids having different charges and different crystalline structures. *Biochim. Biophys. Acta 470*, 303−316.
(46) Silvius, J. R., and Gagne, J. (1984) Calcium-Induced Fusion and Lateral Phase Separations in Phosphatidylcholine-Phosphatidylserine Vesicles: Correlation by Calorimetric and Fusion Measurements. *Biochemistry 23*, 3241−3247.
(47) Frias, M., Benesch, M. G., Lewis, R. N., and McElhaney, R. N. (2011) On the miscibility of cardiolipin with 1,2-diacyl phosphoglycerides: Binary mixtures of dimyristoylphosphatidylethanolamine and tetramyristoylcardiolipin. *Biochim. Biophys. Acta 1808*, 774−783.
(48) Grey, M., Linse, S., Nilsson, H., Brundin, P., and Sparr, E. (2011) Membrane Interaction of α-Synuclein in Different Aggregation States. *J. Parkinson's Dis. 1*, 359−371.
(49) Stanglmaier, S., Hertrich, S., Fritz, K., Moulin, J. F., Haese-Seiller, M., Radler, J. O., and Nickel, B. (2012) Asymmetric distribution of anionic phospholipids in supported lipid bilayers. *Langmuir 28*, 10818−10821.
(50) Pfefferkorn, C. M., Jiang, Z., and Lee, J. C. (2012) Biophysics of α-synuclein membrane interactions. *Biochim. Biophys. Acta 1818*, 162−171.
(51) Mihailescu, M., Vaswani, R. G., Jardon-Valadez, E., Castro-Roman, F., Freites, J. A., Worcester, D. L., Chamberlin, A. R., Tobias, D. J., and White, S. H. (2011) Acyl-chain methyl distributions of liquid-ordered and -disordered membranes. *Biophys. J. 100*, 1455−1462.
(52) Kucerka, N., Tristram-Nagle, S., and Nagle, J. F. (2005) Structure of fully hydrated fluid phase lipid bilayers with monounsaturated chains. *J. Membr. Biol. 208*, 193−202.
(53) Ulmer, T. S., Bax, A., Cole, N. B., and Nussbaum, R. L. (2005) Structure and dynamics of micelle-bound human α-synuclein. *J. Biol. Chem. 280*, 9595−9603.
(54) Varkey, J., Mizuno, N., Hegde, B. G., Cheng, N., Steven, A. C., and Langen, R. (2013) α-Synuclein oligomers with broken helical conformation form lipoprotein nanoparticles. *J. Biol. Chem. 288*, 17620−17630.
(55) Zhu, M., Li, J., and Fink, A. L. (2003) The Association of α-Synuclein with Membranes Affects Bilayer Structure, Stability, and Fibril Formation. *J. Biol. Chem. 278*, 40186−40197.
(56) Haque, F., Pandey, A. P., Cambrea, L. R., Rochet, J. C., and Hovis, J. S. (2010) Adsorption of α-synuclein on lipid bilayers: Modulating the structure and stability of protein assemblies. *J. Phys. Chem. B 114*, 4070−4081.
(57) Jo, E., McLaurin, J., Yip, C. M., St George-Hyslop, P., and Fraser, P. E. (2000) α-Synuclein membrane interactions and lipid specificity. *J. Biol. Chem. 275*, 34328−34334.
(58) Tsui, F. C., Ojcius, D. M., and Hubbell, W. L. (1986) The intrinsic pKa values for phosphatidylserine and phosphatidylethanolamine in phosphatidylcholine host bilayers. *Biophys. J. 49*, 459−468.
(59) Sparr, E., and Olofsson, G. (2013) Ionization constants pKa of cardiolipin. PLOS ONE, In press.
(60) Kates, M., Syz, J. Y., Gosser, D., and Haines, T. H. (1993) pH-dissociation characteristics of cardiolipin and its 2′-deoxy analogue. *Lipids 28*, 877−882.
(61) Zhu, M., Li, J., and Fink, A. L. (2003) The association of α-synuclein with membranes affects bilayer structure, stability, and fibril formation. *J. Biol. Chem. 278*, 40186−40197.
(62) Pandey, A. P., Haque, F., Rochet, J. C., and Hovis, J. S. (2009) Clustering of α-synuclein on supported lipid bilayers: Role of anionic lipid, protein, and divalent ion concentration. *Biophys. J. 96*, 540−551.
(63) Ole, G. M. (2005) *Life: As a matter of fat. The emerging science of lipidomics*, Springer-Verlag, Berlin.

(64) Butterfield, S. M., and Lashuel, H. A. (2010) Amyloidogenic protein-membrane interactions: Mechanistic insight from model systems. *Angew. Chem., Int. Ed. 49*, 5628−5654.
(65) Zakharov, S. D., Hulleman, J. D., Dutseva, E. A., Antonenko, Y. N., Rochet, J. C., and Cramer, W. A. (2007) Helical α-synuclein forms highly conductive ion channels. *Biochemistry 46*, 14369−14379.
(66) Ma, C., Wu, B., and Zhang, G. (2013) Protein-protein resistance investigated by quartz crystal microbalance. *Colloids Surf., B 104*, 5−10.
(67) Sauerbrey, G. (1959) Verwendung Von Schwingquarzen Zur Wagung Dunner Schichten Und Zur Mikrowagung. *Z. Phys. 155*, 206−222.
(68) Vandoolaeghe, P., Rennie, A. R., Campbell, R. A., and Nylander, T. (2009) Neutron reflectivity studies of the interaction of cubic-phase nanoparticles with phospholipid bilayers of different coverage. *Langmuir 25*, 4009−4020.
(69) Martin, R. B. (1963) Deuterated Water Effects on Acid Ionization Constants. *Science 139*, 1198−1203.
(70) Krezel, A., and Bal, W. (2004) A formula for correlating pKa values determined in D_2O and H_2O. *J. Inorg. Biochem. 98*, 161−166.
(71) Covington, A. K., Paabo, M., Robinson, R. A., and Bates, R. G. (1968) Use of the glass electrode in deuterium oxide and the relation between the standardized pD (paD) scale and the operational pH in heavy water. *Anal. Chem. 40*, 700−706.
(72) Nylander, T., Campbell, R. A., Vandoolaeghe, P., Cardenas, M., Linse, P., and Rennie, A. R. (2008) Neutron reflectometry to investigate the delivery of lipids and DNA to interfaces. *Biointerphases 3*, FB64.
(73) Moore, E. B., and Molinero, V. (2011) Structural transformation in supercooled water controls the crystallization rate of ice. *Nature 479*, 506−508.
(74) Armen, R. S., Uitto, O. D., and Feller, S. E. (1998) Phospholipid component volumes: Determination and application to bilayer structure calculations. *Biophys. J. 75*, 734−744.
(75) Petrache, H. I., Tristram-Nagle, S., Gawrisch, K., Harries, D., Parsegian, V. A., and Nagle, J. F. (2004) Structure and fluctuations of charged phosphatidylserine bilayers in the absence of salt. *Biophys. J. 86*, 1574−1586.
(76) Kucerka, N., Holland, B. W., Gray, C. G., Tomberli, B., and Katsaras, J. (2012) Scattering density profile model of POPG bilayers as determined by molecular dynamics simulations and small-angle neutron and X-ray scattering experiments. *J. Phys. Chem. B 116*, 232−239.
(77) Pan, J., Heberle, F. A., Tristram-Nagle, S., Szymanski, M., Koepfinger, M., Katsaras, J., and Kucerka, N. (2012) Molecular structures of fluid phase phosphatidylglycerol bilayers as determined by small angle neutron and X-ray scattering. *Biochim. Biophys. Acta 1818*, 2135−2148.
(78) Quillin, M. L., and Matthews, B. W. (2000) Accurate calculation of the density of proteins. *Acta Crystallogr. D56*, 791−794.